Journal of Materials Chemistry A

PAPER

View Article Online
View Journal | View Issue

Cite this: J. Mater. Chem. A, 2015, 3, 1498

Ge–graphene–carbon nanotube composite anode for high performance lithium-ion batteries

Shan Fang, Laifa Shen, Hao Zheng and Xiaogang Zhang*

Received 22nd August 2014
Accepted 13th November 2014

DOI: 10.1039/c4ta04350b

www.rsc.org/MaterialsA

A Ge–graphene–carbon nanotube composite electrode was constructed by germanium (Ge) nanoparticles anchored on reduced graphene oxide (Ge–RGO) intertwined with carbon nanotubes (CNT). In this unique structure, the graphene sheets improve the electrical conductivity and buffer severe volume changes. Additionally, the CNT mechanically binds together with Ge–RGO to maintain the integrity of the electrodes and stabilize the electric conductive network for the active Ge nanoparticles, leading to better cycling performance. As a result, the designed anode exhibits an outstanding energy capacity up to 863.8 mA h g^{-1} at a current density of 100 mA g^{-1} after 100 cycles and good rate performances of 1181.7, 1073.8, 1005.2, 872.0, 767.6, and 644.8 mA h g^{-1} at current densities of 100, 200, 400, 800, 1600, and 3200 mA g^{-1}, respectively. Our results indicate that the hybrids exhibit considerably improved lithium storage performance.

Introduction

In the past decade, substantial efforts have been devoted to develop rechargeable lithium-ion batteries for large-scale applications such as electric vehicles (EVs) and load-leveling installations on power grids. New generation electrode materials with high energy density and long cycle life have been widely studied to help meet the challenging requirements of these energy storage applications.[1–5] However, existing lithium ion batteries (LIBs) rely on anodes made from graphitic carbon that, at full lithiation, only offer a theoretical capacity nearing 372 mA h g^{-1}, which is unable to satisfy the requirements of increasing mobility and high energy demands.[6] Therefore, the development of alternative anode materials with high energy and high power density for the next generation LIBs is urgently required. Various anode materials with higher specific capacities have been studied in recent years.[7,8] Among them, germanium (Ge) has attracted considerable interest as an anode material for next generation LIBs by virtue of its high theoretical capacity (1600 mA h g^{-1}), good lithium ion diffusivity (400 times faster than in silicon), and high electrical conductivity (104 times higher than silicon).[9,10] Although substituting Ge for graphite and the resulting gain of capacity has been previously explored, it has a major drawback in the form of significant volume expansion (>300%) during Li-ion insertion into Ge. This makes it unstable, leading to internal cracks, delamination from the current collector and increased impedance, which seriously hinder its practical application.[11–14] Various strategies have been followed to solve this problem, and most of them involve the use of nano-sized particles and carbon coating methods.[15–24] Nano-sized particles can withstand mechanical strain during lithium ion insertion/extraction better than bulk and provide shorter path lengths for the transport of lithium ions and electrons.[25,26] Thus, the problems of pulverization and electrical connectivity loss caused by the large volume change of Ge can be weakened to a certain extent. The carbon coating method can protect the surface of the Ge active material from exposure to the electrolyte and form a stable solid electrolyte film (SEI).[27,28] However, due to the high surface-to-volume ratio and high-surface free energy of nano materials, undesirable side reactions and agglomeration can occur easily.[29] With prolonged cycling, the uneven large volume changes of Ge during Li^+ insertion and extraction could destroy the carbon coatings and expose the surface of Ge to the electrolyte. Therefore, serious capacity degradation of Ge can appear during the early cycles.

To further advance the anode performance and stability, two-dimensional (2D) graphene or reduced graphene oxide (RGO), or one-dimensional carbon nanotubes (CNT) are being studied more than other carbon materials, due to their many unusual features. These include superior electrical conductivity, excellent mechanical flexibility, large specific surface area, and high thermal and chemical stability, which can be engineered into a lightweight, robust, and flexible matrix.[30–37] For example, Hwang and co-workers fabricated Ge–MWCNT by anchoring Ge on the surface of electrophoretically pre-deposited MWCNT networks *via* a thermal evaporation process. This nanocomposite electrode showed stable cycling performance and good rate capability.[38] Cho's group directly grew graphene on a

Jiangsu Key Lab of Material and Technology for Energy Conversion, College of Materials Science and Engineering, Nanjing University of Aeronautics and Astronautics, Nanjing, 210016, P. R. China. E-mail: azhangxg@nuaa.edu.cn; Fax: +86 025 52112626; Tel: +86 025 52112902

Ge NW surface by chemical vapor deposition (CVD). The Gr–Ge NW showed an excellent electrochemical performance as anode in a Li ion battery.[39] Lee and co-workers have reported a facile preparation of a Ge–graphene nanocomposite using a low-pressure thermal evaporation approach. The nanocomposite exhibited a high coulombic efficiency of 80.4% in the first cycle and a capacity retention of 84.9% after 400 full cycles in a half cell, along with a high utilization of germanium in the composite and high rate capability.[20] Zhong's group synthesized Ge–graphene by a one-step, aqueous-based method. The germanium–graphene nanocomposite showed a stable cycling performance with a capacity of about 832 mA h g^{-1} after 50 cycles at 0.1 C. The rate capability also improved significantly.[40] However, to date, there has been no research that has attempted to mechanically and electrically bind these nanoscale hybrid materials units together, forming a functional Ge based LIB anode.

In this paper, a comprehensive study was conducted on the Ge-based anode material (namely, Ge–RGO–CNT) consisting of Ge nanoparticles anchored on the surface of RGO and intertwined with CNT to promote the electrochemical performance of Ge based anode material for LIBs. RGO, with its heavily crumpled nature, is a good absorber for accommodating Ge volume changes during the charge and discharge process, and is also electrically conductive, facilitating charge-transfer reactions. The tangled CNT network is expected to provide additional mechanical strength to maintain the integrity of electrodes, forming a continuous 3D electric conductive network and prevent the aggregation of Ge nanoparticles, and eventually result in a better cycling performance. The efficiency of this concept is demonstrated by the facile synthesis of the Ge–RGO–CNT nanocomposite, which shows considerably improved specific capacity, cycling performance, and rate capability in comparison with pristine Ge and Ge–RGO when used as an anode material for LIBs.

Experimental section

Preparation of Ge–RGO–CNT composites

Ge nanoparticles were synthesized according to previous literature.[41] In a typical synthesis, 1.0 mmol $GeBr_2$ and 20 mL oleylamine were added to a 50 mL three-neck flask in air, and bubbled with N_2 gas at ~120 °C for 30 min to remove moisture and oxygen. After heating the mixture at 280 °C for 4 h, a black colloidal solution was obtained. The reaction was allowed to cool to room temperature, following which excess ethanol was added to flocculate the nanoparticles, which were collected by centrifugation at 10 000 rpm for 5 min. After the washing process, the precipitates were treated at 500 °C for 2 h in a furnace under an Ar atmosphere containing 5% (v/v) H_2 to obtain a dark powder. The rate of heating was 2 °C min^{-1}. The Ge–RGO–CNT nanocomposite was prepared by dispersing this material in ethanol solution. First, a 32 mL aqueous solution of GO, which was synthesized from graphite flakes by a modified Hummers method,[42] was vacuum filtered, dried and then ultrasonicated with 50 mL of ethanol for 2 h. Then, 56 mg of the prepared Ge nanoparticles and 8 mg of carbon nanotube (CNT) were added into the solution under magnetic stirring for 1 h to obtain a homogeneous suspension. Following this, the composites were collected by vacuum filtration, washed with ethanol and dried overnight at 60 °C. Finally, reduction in a crucible in a tube furnace at 600 °C for 4 h under 5% (v/v) H_2 atmosphere was carried out to obtain the Ge–RGO–CNT products. The Ge–RGO sample was fabricated for comparison by the same preparation procedure without adding CNT.

Characterization

Morphologies of the samples were characterized by scanning electron microscopy (SEM, HITACHI S-4800) and transmission electron microscopy (TEM, JEOL JEM-2010). The crystal structure was characterized by X-ray diffraction (XRD) (Bruker D8 advance) with Cu Kα radiation over the 2 theta range of 10–80°. Raman spectra were collected using a Renishaw 2000 system with an argon ion laser (514.5 nm) and charge-coupled device detector.

Electrochemical test

Electrochemical evaluations were performed by galvanostatic charge/discharge in a CR2016-type coin cell. 80% active materials, 10% carbon black and 10% polyvinylidene fluoride (PVDF) binder were mixed and dissolved in *N*-methyl pyrrolidone (NMP). Thus, the slurry obtained was coated on a copper foil current collector forming a working electrode. Then, the electrodes were dried overnight in a vacuum oven at 110 °C. The mass of active material loaded on the electrode was ~0.7 mg. The cells were assembled with lithium metal as the counter electrode and polypropylene (PP) film as separator. The electrolytes used were 1 mol L^{-1} $LiPF_6$ solution in a mixture of ethylene carbonate (EC) and dimethyl carbonate (DMC) (1 : 1, by volume). All the cells were assembled inside an argon-filled glove box. Galvanostatic charge/discharge experiments were performed at a voltage between 0.01 and 2.0 V (*vs.* Li/Li^+) using a CT2001A cell test instrument (LAND Electronic Co.). An electrochemical workstation (CHI660) was used to study the cyclic voltammetry (CV) performance in the potential range of 0.05–2.0 V at a scan rate of 0.1 mV s^{-1}. Electrochemical impedance spectroscopy (EIS) was measured in the frequency between 100 kHz and 0.01 Hz and the amplitude was 5 mV.

Results and discussions

The overall synthesis process for the continuous 3D electric conductive network of Ge–RGO–CNT nanocomposite is

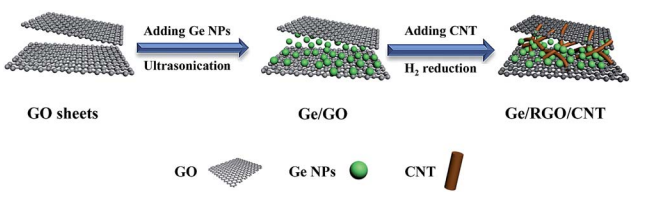

Fig. 1 Schematic illustration of the preparation process of the Ge–RGO–CNT nanocomposite.

schematized in Fig. 1. A solution method based on the reaction between $GeBr_2$ and oleylamine were used to prepare Ge NPs as previously reported.[41] The as-obtained Ge NPs were first heat treated at 500 °C for 2 h under Ar to get a dark powder. They were then added into the ethanol solution of graphene oxide (GO), which was synthesized according to the modified Hummers method starting from graphite powder. Acid-treated carbon nanotubes can be well dispersed in ethanol solutions. The individual CNT are adsorbed onto the surface of GO sheets due to the p-stacking interactions and the reactions of oxygen functionalities such as hydroxyl, carbonyl and carboxyl groups or other defects in the oxidized graphitic structures. Finally, the products were obtained by vacuum filtration and heating at 600 °C for 4 h under Ar containing 5% H_2 in order to reduce GO into RGO. To investigate the structure of the composite, we first performed the scanning electron microscopy (SEM) analysis on the composite samples as shown in Fig. 2. The Ge nanoparticles in both Ge–RGO and Ge–RGO–CNT samples were well wrapped by graphene. Unwrapped Ge nanoparticles were not observed, suggesting high yield of graphene-encapsulated Ge composite in the fabrication process. From Fig. 2c and d, we can easily find the CNT inserted between RGO sheets and Ge nanoparticles, thus preventing Ge nanoparticles from aggregation. This unique nano-structure of the Ge–RGO–CNT not only improves the electronical conductivity of active materials, but also provides the void space to accommodate volume changes of Ge nanoparticles during charge/discharge cycles, maintaining high electronic conductivity of the composite. These hybrid carbon conducting fillers, namely, graphene sheets and CNTs, were employed to achieve the synergy effects of forming extensive 3D conducting networks that cannot be obtained using one type of carbon filler alone.

To further study the morphology of the materials, transmission electron microscopy (TEM) was used to analyze the materials. From the TEM images (Fig. 3a and b), both the Ge NPs and transparent layers can be observed clearly, and the Ge NPs with the diameters in the range of 20–30 nm are uniformly distributed on the graphene substrate, avoiding/weakening the loss of their high active surface area. The images shown in Fig. 3c and d reveal that the individual CNT are placed on the graphene surface together with surrounding Ge nanoparticles, indicating that both the graphene and CNTs in the hybrids are effectively distributed in the Ge–RGO–CNT hybrid sample. Therefore, constructing the RGO–CNT hierarchical structure effectively prevents the stacking of graphene sheets and aggregation of Ge nanoparticles, leading to higher porosity and larger specific surface area to enhance the electrochemical performances of Ge–RGO–CNT. Moreover, the conductive CNT wraps around Ge–RGO to provide an additional electron-transport path in addition to the graphene layer underneath the Ge nanoparticles, and improves the electrode integrity, thus mitigating the destruction of the electric network even under a large volume change during cycling. The high transmission electron microscopy (HRTEM) analysis exhibits the lattice fringe that is indicative of the well-crystallized Ge (Fig. 3e). The calculated interference fringe spacing of Ge is about 0.31 (Fig. 3f), which agrees well with the (111) plane of diamond cubic Ge. The selected-area electron diffraction (SAED) pattern (inset of Fig. 3e) also reveals that the nanoparticles have a diamond cubic structure.

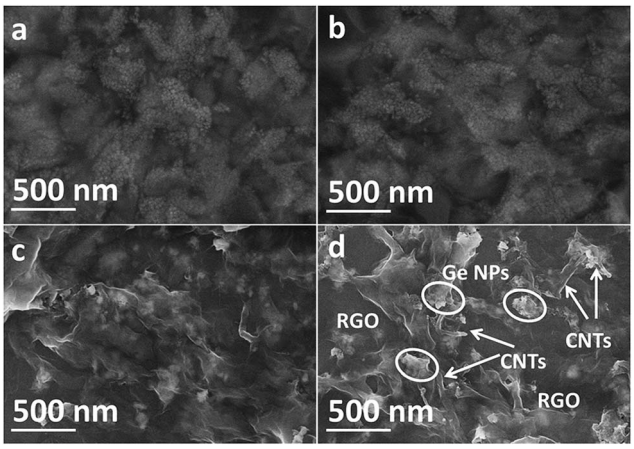

Fig. 2 SEM images of (a and b) Ge–RGO, (c and d) Ge–RGO–CNT nanocomposite.

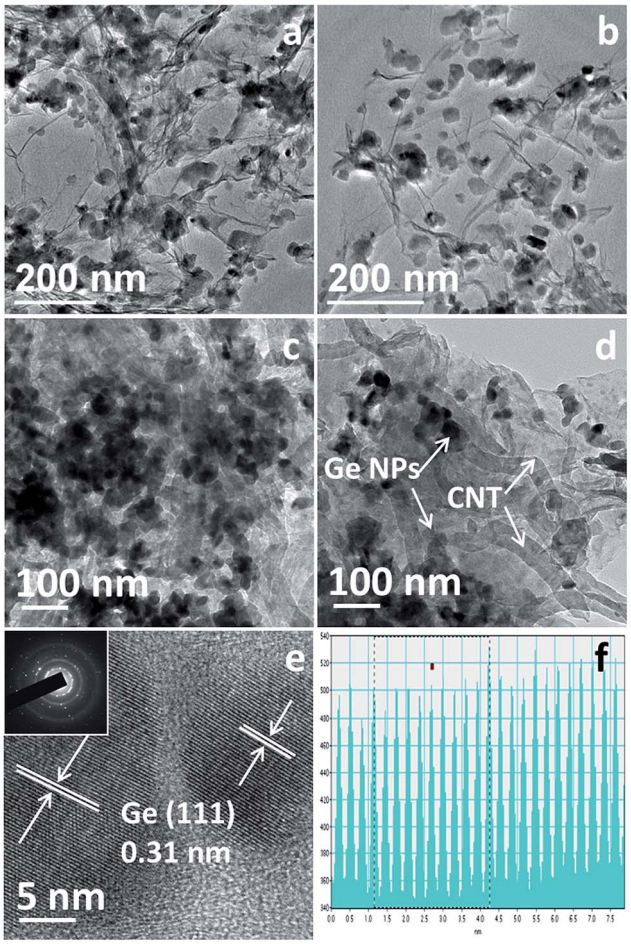

Fig. 3 TEM images of (a and b) Ge–RGO, (c and d) Ge–RGO–CNT nanocomposite. (e and f) HRTEM of Ge nanoparticles inset: selected area SAED pattern for Ge nanoparticles and the correspond calculation of interference fringe spacing.

The crystal structures of the Ge nanoparticles, Ge–RGO and Ge–RGO–CNT samples were characterized by X-ray diffraction (XRD), as shown in Fig. 4a. All the reflection peaks of the samples were well indexed to diamond cubic phase (Ge) (JCPDS card no. 04-0545). There are no peaks corresponding to carbon detected in the pattern, which could be attributed to their overlapping with the (111) peak of germanium at around 27°. To investigate the carbon quality of the synthesized RGO sheets, we obtained the Raman spectrum (Fig. 4b). The RGO exhibits two peaks at around 1348.1 and 1584.9 cm^{-1}, which can be attributed to the D and G bands of carbon, respectively. The D band corresponds to the structural defects and disorder of carbon, whereas the G band corresponds to the stretching vibration mode of graphite crystals. The observed D band is stronger compared to the G band, indicating a largely disordered structure of the obtained RGO.

A series of electrochemical characterizations were carried out to investigate the electrochemical properties of the composite electrodes in a coin type, half cell (2016 type). The electrochemical properties of Ge nanoparticles, Ge–RGO and Ge–RGO–CNT were evaluated and compared (Fig. 5). Fig. 5a shows the charge/discharge voltage profiles of the three samples at a current density of 100 mA g^{-1} in the voltage between 0.01 and 2.0 V. It is evident that the discharge process of the three samples consists of three stages: the first stage is the quick voltage drop, the second stage is the distinct voltage plateau, and the third stage is a gradual decay in potential. A distinct plateau at about 0.3 V can be observed and this can be attributed to the lithium alloying with crystalline Ge nanoparticles.[43] The initial discharge and charge capacities of Ge nanoparticles are 1765.1 and 696.4 mA h g^{-1}, respectively, corresponding to a coulombic efficiency (CE) of 39.4%. The relatively low initial CE of pristine Ge can be attributed to the drastic volume changes and the loss of electric contact between Ge nanoparticles, which in turn leads to a large, irreversible capacity. The charge/discharge curves of Ge–RGO are also shown in Fig. 5a. In addition to the potential plateau at 0.3 V, an obvious step can also be observed between 0.70 and 0.30 V, which is attributed to the solid electrolyte interphase (SEI) formed by the irreversible decomposition of the electrolyte on the surface of the electrode material.[44,45] The initial discharge and charge capacity of Ge–RGO are 1563.2 and 1208.2 mA h g^{-1}, respectively, corresponding to a CE of 77.3%. It should be noted that the CE is improved after adding RGO even if an obvious irreversible SEI formation process is observed between 0.70 and 0.30 V, which can be attributed to the volume buffer effect of reduced graphene oxide and the better electric conductive network. The Ge–RGO–CNT (Fig. 5a) shows a similar charge/discharge characteristic to that of Ge–RGO. The initial discharge and charge capacities of Ge–RGO–CNT are 1602.4 and 1277.4 mA h g^{-1}, respectively, and the CE is up to 79.7%. Apparently, the 3D conducted network structure results in profound improvement in electrochemical performance.

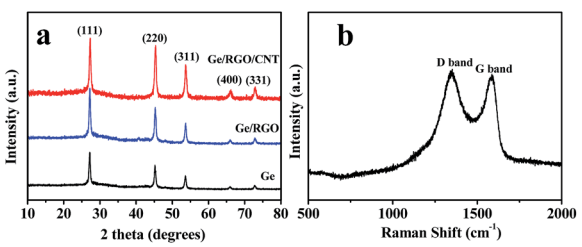

Fig. 4 (a) XRD patterns of Ge, Ge–RGO and Ge–RGO–CNT. (b) Raman spectrum of the as-prepared RGO sheets.

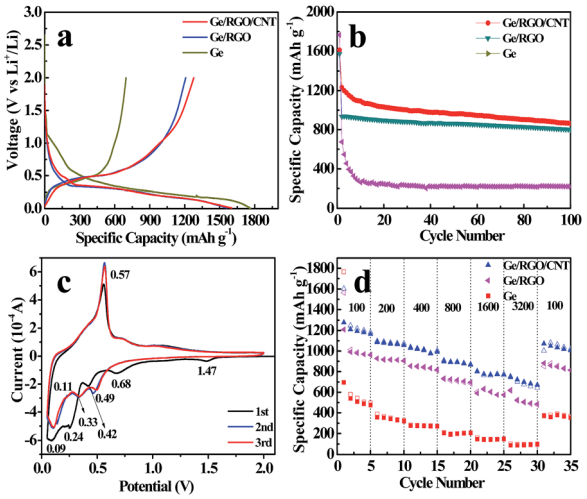

Fig. 5 (a) Charge/discharge voltage profiles of pure Ge, Ge–RGO and Ge–RGO–CNT nanocomposite at a rate of 100 mA g^{-1}. (b) Cycling performance of the three different samples at a current density of 100 mA g^{-1}. (c) Cyclic voltammetry curves of Ge–RGO–CNT between 2.0 and 0.05 V with a scan rate of 0.1 mV s^{-1}. (d) Rate performance of pure Ge, Ge–RGO and Ge–RGO–CNT nanocomposite electrodes at different current rates.

The cycling behaviors for the three different samples are shown in Fig. 5b. Here, all capacities were calculated on the basis of the total weight of composite material including Ge, graphene and CNT. The discharge capacity of the pristine Ge electrode rapidly decreased to 220 mA h g^{-1} after 100 cycles at a current density of 100 mA g^{-1}. This may originate from the serious pulverization of the Ge, during which the SEI layer continuously ruptures and reforms, consuming Li^+. In comparison, the 3D conductive network formed by graphene and CNT grafted Ge composites still retains a specific discharge capacity of about 863.8 mA h g^{-1}. It is worthwhile to point out that even without adding CNT, the composites of Ge–RGO still show improved cycle performance compared to bare Ge nanoparticles, but a worse cycle life performance than that of the Ge–RGO–CNT. This result may be ascribed to the three-dimensional electric conductive network, which improves the electric conductivity, buffers the volume change and the CNTs work together to achieve high electrode integrity. In order to confirm the reaction mechanism of alloying/de-alloying for Ge–RGO–CNT, cyclic voltammetry (CV) was conducted on the cell with Ge–RGO–CNT at ambient temperature in the range of 0.05–2.0 V at a scan rate of 0.1 mV s^{-1}. Li metal was used as the counter electrode. The CV curves of the first three cycles are shown in Fig. 5c. Two extra reduction peaks at 1.47 and 0.68 V were observed in the first scanning cycle, which could be

associated with the formation of a solid electrolyte interphase (SEI) layer. The other three peaks are present at 0.42, 0.24 and 0.09 V, indicating the complete reduction process. However, both of them disappear after the second cycle,[46] and new, well-defined peaks were observed at 0.49, 0.33, and 0.11 V.[47,48] These are stable, detectable and suggest a multi-step lithium insertion mechanism as the electrochemical reaction of Ge with lithium exhibits multiple peaks during repeated lithiation, indicating the presence of successive Li phase transformations, as follows: Ge → Li_9Ge_4 → Li_7Ge_2 → $Li_{15}Ge_4$ → $Li_{22}Ge_5$.[48] Moreover, the positions and intensities of the redox peaks remain unchanged during the second and third cycles, suggesting that the Ge–RGO–CNT nanocomposite electrode has an excellent electrochemical reversibility.

The fast discharge/charge further validates the reliability of RGO–CNT conductive network during a rapid substantial expansion and contraction for Ge nanoparticles. The rate performances of Ge nanoparticles, Ge–RGO, Ge–RGO–CNT at a current density of 100–3200 mA g^{-1} are compared in Fig. 5d. Remarkably, as the discharge/charge rate increased from 100 to 3200 mA g^{-1}, the capacity of pure Ge decreased steeply, whereas that of the Ge–RGO mixture decreased relatively slowly at the same rate. Moreover, by introducing a conductive CNT, which was inserted into Ge–RGO to form a 3D conductive network structure, the Ge–RGO–CNT hybrid nanostructures exhibited the highest rate capacity among the three samples. It is indeed noteworthy that the capacity (754.1 mA h g^{-1}) obtained by Ge–RGO–CNT nanocomposite at a current density of 3200 mA g^{-1} is higher than that obtained at a current density of 100 mA g^{-1} for the bare Ge (496.2 mA h g^{-1}) and 1600 mA g^{-1} for the Ge–RGO mixture (686.3 mA h g^{-1}). Our Ge–RGO–CNT hybrid nanostructures have better electrochemical properties than graphene-wrapped Ge nanoparticle[49] and germanium–graphene nanocomposite synthesized by reduced GeO_2.[40]

To confirm the enhanced electrical conductivity of the Ge–RGO–CNT in comparison with Ge–RGO and Ge nanoparticles, we performed electrochemical impedance spectroscopy (EIS) measurements on the three electrodes after running 100 cycles at the same current density. The EIS spectra for the three electrodes typically consist of a depressed semicircle in the high-frequency region and an inclined line in the low-frequency region as shown in Fig. 6a. The depressed semicircle mainly consists of the interfacial charge transfer impedance (R_{ct}) at the medium-to-high frequency range, although the high-frequency SEI film impedance (R_{SEI}) also contributes to it. The inclined line corresponds to the lithium ion diffusion impedance. Apparently, the Ge–RGO–CNT electrode shows a considerably lower charge-transfer resistance R_{ct} and R_{SEI} than the Ge–RGO and Ge NPs electrodes, indicating faster Li-ion migration through the SEI film and faster charge-transfer reaction for the Ge–RGO–CNT anode. This results in a better rate capability and higher reversible capacity of Ge–RGO–CNT in comparison with the pure Ge nanoparticles, which is similar to the phenomenon found in many other graphene-based hybrids. The characteristics of the Ge–RGO–CNT anode in LIBs are elucidated by the schematic diagram (Fig. 6b). The high specific capacity and superior rate capability of Ge–RGO–CNT are closely related to its unique structure, which favors both the ion and electron transportation in the LIBs. First, the small size (20–30 nm) and uniform distribution of germanium nanoparticles between the graphene and the CNT interconnected network promote fast lithium ion diffusion and further improve the conductivity of the composite. Second, the CNT attached on the surface of graphene reduces the π–π interaction between graphene sheets resulting from steric hindrance. This leads to a reduction in the degree of restacking of RGO and consequently the retention of large active contact area between the electrode and electrolyte, which leads to a decrease of the current density per unit surface area and an increase in the charge/discharge rate. Third, the high structural stability of the composite material owing to the synergistic effects of the graphene sheets and CNTs that intertwine the germanium nanoparticles, thereby protecting them from peeling off and further pulverization. The CNT inserted in the RGO sheets could provide a support for anchoring well-dispersed Ge, the three-dimensional interconnected network possesses continuous electronic conductivity and Li diffusivity, which are favorable in terms of its LIB performance.

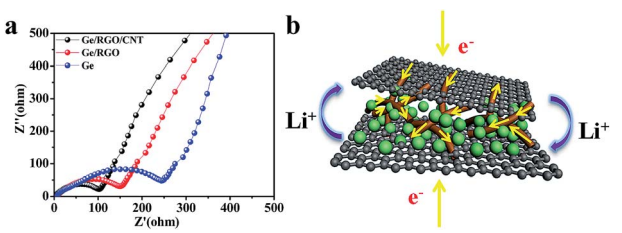

Fig. 6 (a) Nyquist plots of the electrodes of Ge, Ge–RGO and Ge–RGO–CNT nanocomposites. (b) Schematic drawing of Ge–RGO–CNT nanocomposites electrode.

Conclusions

In summary, we have developed a facile route to form a 3D conductive network structure as an advanced anode material for high-power LIBs. The Ge nanoparticles are uniformly dispersed on the surface of graphene and carbon nanotubes, which serve as the ideal host for fast and efficient lithium storage. The highly conductive 3D networks formed by the interlaced carbon nanotubes are intimately embedded or attached on the graphene, which serves as a highly conductive substrate that is beneficial to the high-rate performance. At the same time, the large surface area provides more reaction sites and lower activation energy for lithium ion insertion/extraction. It is believed that such hybrid materials composed of nanoactive particles (0D), carbon nanotubes (1D), and graphene (2D) with designed structure and varied properties will be useful in energy storage and other important applications.

Acknowledgements

This work was supported by the National Basic Research Program of China (973 Program) (no. 2014CB239701), National Natural Science Foundation of China (no. 21173120, 51382116),

Natural Science Foundation of Jiangsu Province (BK2011030), and Fundamental Research Funds for the Central Universities of NUAA (NP2014403).

Notes and references

1 X. Zhou, Z. Dai, S. Liu, J. Bao and Y. G. Guo, *Adv. Mater.*, 2014, **26**, 3943–3949.
2 L. Zhang, H. B. Wu, B. Liu and X. W. Lou, *Energy Environ. Sci.*, 2014, **7**, 1013–1017.
3 Z. Liang, G. Zheng, W. Li, Z. W. Seh, H. Yao, K. Yan, D. Kong and Y. Cui, *ACS Nano*, 2014, **8**, 5249–5256.
4 M. S. Park, E. Park, J. Lee, G. Jeong, K. J. Kim, J. H. Kim, Y. J. Kim and H. Kim, *ACS Appl. Mater. Interfaces*, 2014, **6**, 9608–9613.
5 X. Huang, H. Yu, J. Chen, Z. Lu, R. Yazami and H. H. Hng, *Adv. Mater.*, 2014, **26**, 1296–1303.
6 M. Armand and J. M. Tarascon, *Nature*, 2008, **451**, 652–657.
7 M. J. Armstrong, C. O'Dwyer, W. J. Macklin and J. D. Holmes, *Nano Res.*, 2014, **7**, 1–62.
8 B. L. Ellis, P. Knauth and T. Djenizian, *Adv. Mater.*, 2014, **26**, 3368–3397.
9 G. Cui, L. Gu, L. Zhi, N. Kaskhedikar, P. A. van Aken, K. Muellen and J. Maier, *Adv. Mater.*, 2008, **20**, 3079–3083.
10 K. H. Seng, M.-H. Park, Z. P. Guo, H. K. Liu and J. Cho, *Angew. Chem., Int. Ed.*, 2012, **51**, 5657–5661.
11 X. H. Liu, Y. Liu, A. Kushima, S. Zhang, T. Zhu, J. Li and J. Y. Huang, *Adv. Energy Mater.*, 2012, **2**, 722–741.
12 C. K. Chan, H. Peng, G. Liu, K. McIlwrath, X. F. Zhang, R. A. Huggins and Y. Cui, *Nat. Nanotechnol.*, 2008, **3**, 31–35.
13 L. Y. Beaulieu, K. W. Eberman, R. L. Turner, L. J. Krause and J. R. Dahn, *Electrochem. Solid-State Lett.*, 2001, **4**, A137–A140.
14 B. Key, R. Bhattacharyya, M. Morcrette, V. Seznec, J. M. Tarascon and C. P. Grey, *J. Am. Chem. Soc.*, 2009, **131**, 9239–9249.
15 T. Kennedy, E. Mullane, H. Geaney, M. Osiak, C. O'Dwyer and K. M. Ryan, *Nano Lett.*, 2014, **14**, 716–723.
16 C. H. Kim, H. S. Im, Y. J. Cho, C. S. Jung, D. M. Jang, Y. Myung, H. S. Kim, S. H. Back, Y. R. Lim, C. W. Lee, J. Park, M. S. Song and W. I. Cho, *J. Phys. Chem. C*, 2012, **116**, 26190–26196.
17 Y. D. Ko, J. G. Kang, G. H. Lee, J. G. Park, K. S. Park, Y. H. Jin and D. W. Kim, *Nanoscale*, 2011, **3**, 3371–3375.
18 H. Lee and J. Cho, *Nano Lett.*, 2007, **7**, 2638–2641.
19 L. Li, K. H. Seng, C. Feng, H. K. Liu and Z. Guo, *J. Mater. Chem. A*, 2013, **1**, 7666–7672.
20 J. G. Ren, Q. H. Wu, H. Tang, G. Hong, W. Zhang and S. T. Lee, *J. Mater. Chem. A*, 2013, **1**, 1821–1826.
21 C. Wang, J. Ju, Y. Yang, Y. Tang, J. Lin, Z. Shi, R. P. S. Han and F. Huang, *J. Mater. Chem. A*, 2013, **1**, 8897–8902.
22 J. Wang, J. Z. Wang, Z. Q. Sun, X. W. Gao, C. Zhong, S. L. Chou and H. K. Liu, *J. Mater. Chem. A*, 2014, **2**, 4613–4618.
23 Y. Xiao, M. Cao, L. Ren and C. Hu, *Nanoscale*, 2012, **4**, 7469–7474.
24 G. Jo, I. Choi, H. Ahn and M. J. Park, *Chem. Commun.*, 2012, **48**, 3987–3989.
25 H. Wu and Y. Cui, *Nano Today*, 2012, **7**, 414–429.
26 X. L. Wu, Y. G. Guo and L. J. Wan, *Chem.–Asian J.*, 2013, **8**, 1948–1958.
27 K. Karki, Y. Zhu, Y. Liu, C. F. Sun, L. Hu, Y. Wang, C. Wang and J. Cumings, *ACS Nano*, 2013, **7**, 8295–8302.
28 M. E. Stournara, Y. Qi and V. B. Shenoy, *Nano Lett.*, 2014, **14**, 2140–2149.
29 B. Jang, M. Park, O. B. Chae, S. Park, Y. Kim, S. M. Oh, Y. Piao and T. Hyeon, *J. Am. Chem. Soc.*, 2012, **134**, 15010–15015.
30 H. Gwon, H.-S. Kim, K. U. Lee, D.-H. Seo, Y. C. Park, Y.-S. Lee, B. T. Ahn and K. Kang, *Energy Environ. Sci.*, 2011, **4**, 1277–1283.
31 L. Hu, J. W. Choi, Y. Yang, S. Jeong, F. La Mantia, L. F. Cui and Y. Cui, *Proc. Natl. Acad. Sci. U. S. A.*, 2009, **106**, 21490–21494.
32 X. Peng, L. Peng, C. Wu and Y. Xie, *Chem. Soc. Rev.*, 2014, **43**, 3303–3323.
33 J. Yan, T. Wei, Z. J. Fan, W. Z. Qian, M. L. Zhang, X. D. Shen and F. Wei, *J. Power Sources*, 2010, **195**, 3041–3045.
34 W. J. Lee, T. H. Hwang, J. O. Hwang, H. W. Kim, J. Lim, H. Y. Jeong, J. Shim, T. H. Han, J. Y. Kim, J. W. Choi and S. O. Kim, *Energy Environ. Sci.*, 2014, **7**, 621–626.
35 W. Wang, S. Guo, M. Penchev, I. Ruiz, K. N. Bozhilov, D. Yan, M. Ozkan and C. S. Ozkan, *Nano Energy*, 2013, **2**, 294–303.
36 B. Zhang, Q. B. Zheng, Z. D. Huang, S. W. Oh and J. K. Kim, *Carbon*, 2011, **49**, 4524–4534.
37 J. D. Ocon, J. K. Lee and J. Lee, *Applied Chemistry for Engineering*, 2014, **25**, 1–13.
38 I. S. Hwang, J. C. Kim, S. D. Seo, S. Lee, J. H. Lee and D. W. Kim, *Chem. Commun.*, 2012, **48**, 7061–7063.
39 H. Kim, Y. Son, C. Park, J. Cho and H. C. Choi, *Angew. Chem., Int. Ed.*, 2013, **52**, 5997–6001.
40 C. Zhong, J.-Z. Wang, X.-W. Gao, D. Wexler and H.-K. Liu, *J. Mater. Chem. A*, 2013, **1**, 10798–10804.
41 D. J. Xue, S. Xin, Y. Yan, K. C. Jiang, Y. X. Yin, Y. G. Guo and L. J. Wan, *J. Am. Chem. Soc.*, 2012, **134**, 2512–2515.
42 W. S. Hummers and R. E. Offeman, *J. Am. Chem. Soc.*, 1958, **80**, 1339.
43 C. K. Chan, X. F. Zhang and Y. Cui, *Nano Lett.*, 2008, **8**, 307–309.
44 J. Graetz, C. C. Ahn, R. Yazami and B. Fultz, *J. Electrochem. Soc.*, 2004, **151**, A698–A702.
45 Y. M. Lee, J. Y. Lee, H.-T. Shim, J. K. Lee and J.-K. Park, *J. Electrochem. Soc.*, 2007, **154**, A515–A519.
46 W. Li, J. Zheng, T. Chen, T. Wang, X. Wang and X. Li, *Chem. Commun.*, 2014, **50**, 2052–2054.
47 J. Wang, N. Du, H. Zhang, J. Yu and D. Yang, *J. Mater. Chem.*, 2012, **22**, 1511–1515.
48 B. Laforge, L. Levan-Jodin, R. Salot and A. Billard, *J. Electrochem. Soc.*, 2008, **155**, A181–A188.
49 J. Cheng and J. Du, *CrystEngComm*, 2012, **14**, 397–400.